Lithium intercalation into WO_3 and the phase diagram of Li_xWO_3

Q. Zhong, J. R. Dahn,* and K. Colbow
Department of Physics, Simon Fraser University, Burnaby, British Columbia, Canada V5A 1S6
(Received 17 January 1992)

We report studies of the electrochemical intercalation of lithium in WO_3 powder and in polycrystalline evaporated WO_3 films. Electrochemical cells with beryllium x-ray windows were used to study the structure changes in the WO_3 host *in situ*. Rietveld profile refinement was used to analyze the x-ray-diffraction patterns of Li_xWO_3 after correcting for the absorption of the beryllium window. Upon the intercalation of Li, the monoclinic structure of WO_3 proceeds to higher and higher symmetry. First a first-order phase transition to a tetragonal phase with $x \sim 0.1$ in Li_xWO_3 occurs. Then another first-order phase transition to a cubic phase with $x \sim 0.36$ occurs. The cubic phase can accommodate further Li, up to a maximum of about $x=0.5$. All the phase transitions can be reversed, although some hysteresis is observed; upon complete deintercalation, monoclinic WO_3 is recovered. We report the structural changes, prove that the transitions are first order, and give a phase diagram for Li_xWO_3 as a function of x. Our results suggest that the formation of the tetragonal phase upon intercalation of Li in WO_3 is responsible for the electrochromatic properties of crystalline Li_xWO_3, and that conventional interpretations that ignore the existence of this phase are most likely in error.

INTRODUCTION

The intercalation of lithium in tungsten trioxide (WO_3) has been studied for many years.[1–4] Much of this work focused on the use of Li_xWO_3, prepared in an electrochemical cell, as an electrochromic. The success of such a device depends critically on the reversibility of the intercalation of Li in WO_3. We were surprised to find that no detailed studies of the structural changes occurring during the intercalation or deintercalation of Li in WO_3 have been made (to our knowledge). Therefore, we decided to make such a study to probe the reversibility of Li intercalation in WO_3.

In this work, lithium intercalation in WO_3 powders and polycrystalline films are reported. We studied both because films are conventionally used in electrochromic devices while our expertise is best suited to the study of powders. Nevertheless, our data on films are of high quality and are similar to the results on the powders.

Using the electrochemical methods, lithium was intercalated into the WO_3 powders and the films, and using *in situ* x-ray diffraction,[5,6] the phase changes in the intercalated Li_xWO_3 were identified from the voltage curves and the x-ray data. The voltage of Li/Li_xWO_3 electrochemical cells measures the chemical potential of lithium in the Li_xWO_3.[7] Since the chemical potentials of the components of coexisting phases (which occur at first-order transitions) are the same as the voltage, $V(x)$, of a Li battery plotted vs x in Li_xWO_3, shows a plateau when two phases coexist. Such plateaus can be directly used to help determine phase-diagram information. Furthermore, the derivative, $-dx/dV$, shows peaks at the voltages and the compositions where the coexisting phases occur. Combining these electrochemical methods with *in situ* x-ray diffraction[8] gives a very powerful method for determining the phase diagram of intercalation compounds[9] which we apply here to Li_xWO_3.

The crystal structure of WO_3 is monoclinic at room temperature, with unit-cell dimensions: $a_M=7.306$ Å, $b_M=7.540$ Å, $c_M=7.692$ Å, and $\beta=90.881°$.[10] There are 8 tungsten and 24 oxygen atoms in each unit cell. (Since β is close to 90°, the structure is pseudo-orthorhombic.) The structure is related to the cubic ReO_3 structure which has metal atoms on the corners of a simple-cubic lattice and oxygen atoms centered on every edge. As we will see, when Li intercalates into Li_xWO_3, the structure becomes successively more simple as x increases. Figure 1 shows schematically the relation between the monoclinic cell of WO_3, the tetragonal cell of $Li_{0.1}WO_3$, and cubic (ReO_3-like) cell of $Li_{0.5}WO_3$.

EXPERIMENTS

The WO_3 powder used here was prepared by heating H_2WO_4 (99.5%, Aldrich) at 400 °C in air for 12 h accord-

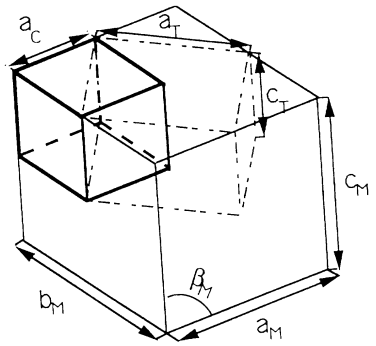

FIG. 1. The relations of tetragonal and cubic-unit cells to the monoclinic unit cell.

ing to the following reaction:

$$H_2WO_4 \xrightarrow{\text{heated}} WO_3 + H_2O \ . \quad (1)$$

H_2WO_4 begins to decompose at about 200 °C and WO_3 is obtained at above 250 °C.[11] Electrodes were prepared from this WO_3 powder using the methods described previously.[12] Typical electrodes had an active mass of 20 mg, a coverage of 14 mg/cm^2 and a thickness of about 100 μm. The WO_3 films studied were evaporated on Al foil or on a Be foil substrate under a vacuum of about 1×10^{-5} Torr. The as-evaporated WO_3 films were amorphous and became polycrystalline after subsequent annealing in air at 400 °C for about 2 h. These WO_3 films were then directly used as electrodes.

Two-electrode electrochemical cells were used to intercalate Li in the WO_3 powder or into the film. Li foil (Lithium Corporation of America) was used as the anode and WO_3 powder electrodes or WO_3 film electrodes as the cathode. The electrolyte was a 1 molar solution of $LiClO_4$ dissolved in a 50:50 volume mixture of propylene carbonate and ethylene carbonate. The $LiClO_4$ salt was vacuum dried at 80 °C for 24 h and the solvents were vacuum distilled prior to use.

Two types of electrochemical cells were used. Hermetically sealed test cells of the type described in Ref. 13 were used to determine the voltage, $V(x)$, of Li/Li_xWO_3 cells. Cells with Be x-ray windows[8] (called x-ray cells here) were used to measure the structural changes in Li_xWO_3 *in situ* as x was changed by charging and discharging the cells. Cu $K\alpha$ radiation was used in all x-ray measurements. Our diffractrometer uses the Bragg-Brentano geometry and has a diffracted beam monochromator.

To determine $V(x)$ and $-dx/dV$, cells were charged and discharged with constant currents between fixed voltage limits. The temperature of the cell was maintained constant in a thermostat to ±0.1 °C. Changes in x are calculated from the cathode mass, the constant current, and the time of current flow. For a 20-mg electrode, a current of 23 μA gives a change $\delta x=1$ in Li_xWO_3 in 100 h. We call this current a 100-h rate for that electrode. Data were measured whenever V changed by 0.005 V.

Two types of *in situ* x-ray experiments were carried out. A constant current was applied to an x-ray cell while a sequence of x-ray-diffraction profiles were continuously measured. This method allows for the rapid collection of data, but if the current is too large, nonequilibrium measurements are obtained. We used currents corresponding to a change $\delta x=1$ in 100 or 200 h where nonequilibrium effects are small. Alternatively, the cell voltage was fixed for about 24 h until the cell current decayed to a few microamperes; an x-ray profile was then collected of the equilibrium cathode.

X-ray patterns were analyzed by Rietveld profile refinement.[14–17] The absorption from the beryllium window of the x-ray cell is angle dependent because of the Bragg-Brentano $(\theta,2\theta)$ geometry we use. Before using the Rietveld program, the recorded intensity (I_r) from the x-ray cell was corrected using

$$I_o = I_r \exp(2\mu l/\sin\theta) \ , \quad (2)$$

where I_o is the diffracted intensity without beryllium absorption, μ is the absorption coefficient of the beryllium, l is the thickness of beryllium foil, and θ is the diffraction angle. One measure of the success of the refinement is the Bragg R_B factor defined as

$$R_B = \frac{\sum_{(h,k.l)} |I_o(h,k,l) - I_c(h,k,l)|}{\sum_{(h,k,l)} I_o(h,k,l)} \ , \quad (3)$$

where $I_o(h,k,l)$ is the observed peak (h,k,l) intensity and $I_c(h,k,l)$ the calculated peak (h,k,l) intensity. The sum goes over all (h,k,l) peaks observed.

RESULTS

Figures 2(a) and 2(b) show the charge and discharge curves for Li/WO_3 cells with film and powder electrodes, respectively. Both materials have two plateaus during their discharge (intercalating Li) process. It will be proved later in this paper that the first plateau near 2.75 V during discharge corresponds to coexistence between monoclinic Li_xWO_3 and tetragonal $Li_{0.1}WO_3$. The second plateau near 2.5 V during discharge corresponds to coexistence between tetragonal $Li_{0.1}WO_3$ and cubic $Li_{0.36}WO_3$. The sloping regions in $V(x)$ near 3.0, 2.7 and 2.2 V correspond to three single-phase regions: monoclinic, tetragonal, and cubic in Li_xWO_3. The phase transitions are not as obvious during charge as during discharge, but are clearly observed when $-dx/dV$ is

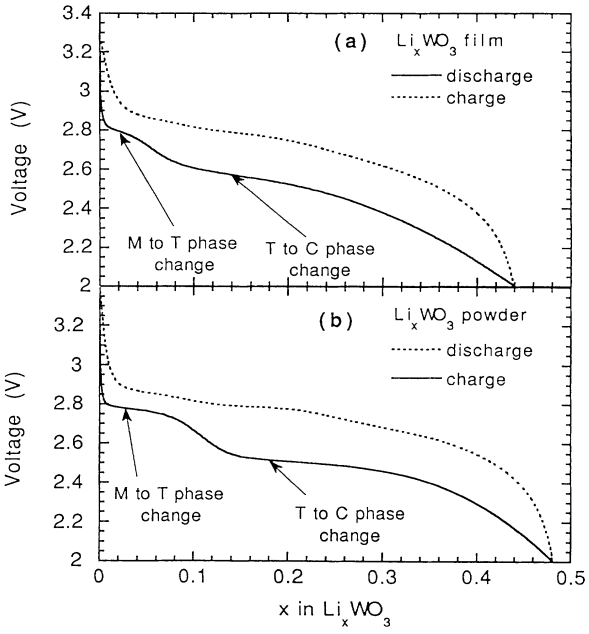

FIG. 2. (a) Voltage vs x for a Li/WO_3 film cell measured at 30 °C. (b) Voltage vs x for a Li/WO_3 powder cell. The solid curve is for the discharge of the cell and the dashed curve is for the charge of the cell. Two plateaus on the discharge curve correspond to the monoclinic (M) to tetragonal (T) phase change, and the tetragonal (T) to cubic (C) phase change.

plotted versus V. Figures 3(a) and 3(b) show $-dx/dV$ calculated from the data of Fig. 2. The derivative is obtained simply by taking $-\delta x/\delta V$ for adjacent data points. The peaks in Fig. 3 correspond to the plateaus in Fig. 2 and thus to the coexisting phase regions in Li_xWO_3. The features in Figs. 2 and 3 which correspond to the phase transitions are sharper for the powder. Presumably the crystallite size of the powder grains is larger than that of the grains in the film. Since finite-size effects are known to broaden first-order transition, we feel that the difference in crystallite size may explain the differences between the powder and the film. The range of stability of the three single phases, monoclinic, tetragonal, and cubic, are also indicated in Fig. 3.

The peaks in $-dx/dV$ suggest that Li_xWO_3 undergoes two reversible phase transitions during discharge and during charge. The broad peak observed near 2.65 V during charge is not associated with a phase transition but corresponds to capacity associated with deintercalation of Li from a single phase. We now report *in situ* x-ray results which show what these transitions and single-phase regions are. Since $V(x)$ and $-dx/dV$ vs V for the WO_3 powder and the WO_3 film are almost the same, the results obtained from Li_xWO_3 powder will be presented and the results obtained from the film will be only quoted for comparison.

Figure 4 shows the x-ray-diffraction pattern for our WO_3 powder. Since a_M, b_M, and c_M all differ in length, the peaks (200), (020), and (002) near 23° all appear at a different scattering angle. Figure 5 shows the x-ray profile obtained from an *in situ* x-ray cell discharged to 2.7 V with $x=0.095$ in Li_xWO_3. The triplet of peaks at 23° in Fig. 4 is now a doublet. This suggests that two of

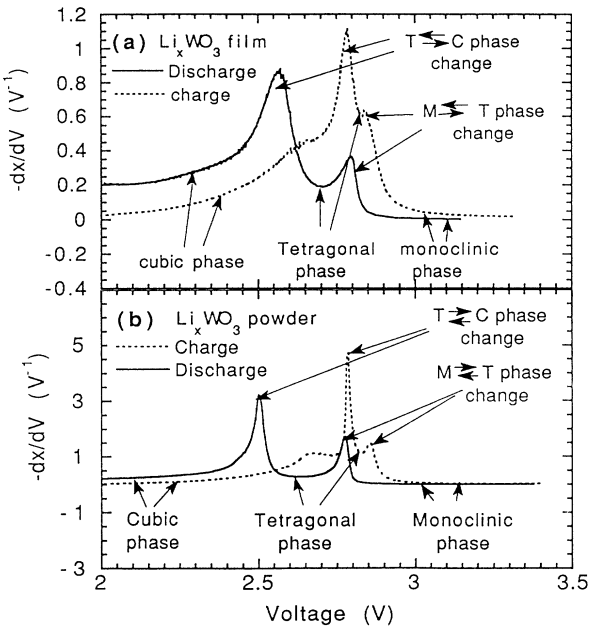

FIG. 3. (a) Derivative $-(dx/dV)_T$ vs V computed from data of Fig. 2(a). The derivative data in (b) correspond to the data of the WO_3 powder cell from Fig. 2. (b) The peaks in the derivative correspond to the plateaus in Fig. 2.

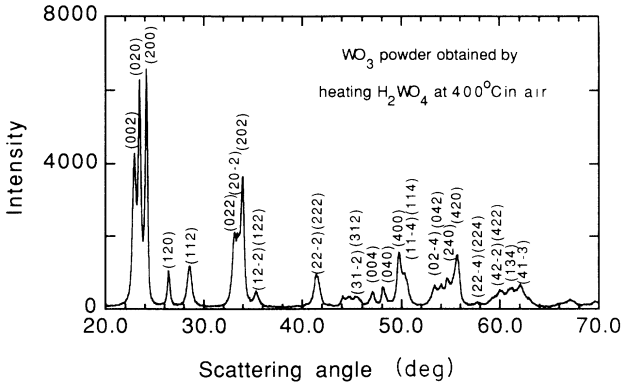

FIG. 4. X-ray diffraction pattern for WO_3 powder obtained by heating H_2WO_3 at 400 °C in air. The Miller index is shown.

the cell axes are now equivalent. We were able to index the pattern successfully using a tetragonal unit cell and proceeded to refine the structure in space group $P4/nmm\text{-}D_{4h}^7$. The refinement was successful giving $R_B=0.048$; Fig. 5 shows that the data and the calculation after refinement are in good agreement. With reference to Fig. 1, $c_T\sim\frac{1}{2}c_M$ and $a_T\sim\frac{1}{2}\sqrt{(a_M^2+b_M^2)}$. We measured $c_T=3.844$ Å and $a_T=5.203$ Å. Table I gives the final results of the refinement. Similar results were obtained for a Li/Li_xWO_3 cell with a film electrode. A cell fixed at 2.70 V gave $x=0.05$ in Li_xWO_3 (the value of x for the tetragonal phase is smaller for the film compared to the powder—see Fig. 2) and could be refined using the same tetragonal structure as the powder except with $a_T=5.221$ Å and $c_T=3.862$ Å.

The x-ray cell with the powder electrode was discharged to 2.0 V which corresponded to $x=0.48$ in Li_xWO_3. Figure 6 shows the diffraction data for the cell. The doublet of peaks near 23° in the tetragonal phase (Fig. 5) is now seen to be a single peak suggesting all three cell axes are equivalent. We were able to successfully index the pattern assuming a cubic structure with

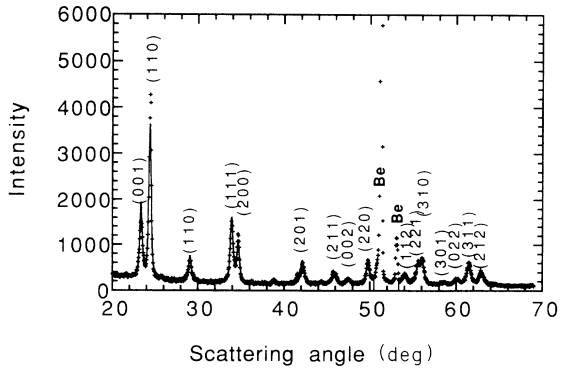

FIG. 5. X-ray-diffraction profile refinement for tetragonal Li_xWO_3 powder in an x-ray cell at $V=2.7$ V; $x=0.095$ in Li_xWO_3. + + + are the x-ray data and the solid line (——) is the calculated profile. The structure parameters used in the calculation were from Table I. Beryllium peaks were excluded from the calculation.

TABLE I. Structure parameters for the tetragonal Li_xWO_3 powder. x in Li_xWO_3: 0.095; space group: $P4/nmm$; cell dimensions: $a_T=5.203$ Å, $c_T=3.844$ Å; refined R factor: 0.048; and origin at $2/m$.

	x	y	z	B
W1	0.25	0.25	0.432	1.0
W2	0.75	0.75	0.568	1.0
O1	0.25	0.25	0.932	4.8
O2	0.75	0.75	0.068	4.8
O3	0.00	0.00	0.50	4.8
O4	0.50	0.50	0.50	4.8
O5	0.50	0.00	0.50	4.8
O6	0.00	0.50	0.50	4.8

$a_C=3.729$ Å. Refinement in $Pm3m$ was successful giving a Bragg R factor of $R_B=0.037$. Table II gives the results of the refinement. With reference to Fig. 1, we expect $a_C\sim\frac{1}{2}(a_M+b_M+c_M)/3$ as observed. The positions of the W and O atoms in $Li_{0.48}WO_3$ are the same as the Re and O atoms in ReO_3. The cubic phase was also found in a Li/Li_xWO_3 cell with a film electrode discharged to 2.0 V ($x=0.44$). The refined results were similar to those for the powder and the lattice constant was 3.726 Å for the film.

It remains to determine how the phase transitions between the monoclinic and tetragonal phases and between the tetragonal and cubic phases occur. An *in situ* x-ray experiment was performed to analyze the monoclinic ↔ tetragonal phase transitions in Li_xWO_3. Figure 7(a) shows the charge and discharge curves for this *in situ* x-ray cell. Figure 7(b) shows the x-ray profiles taken at the points *a*, *b*, *c*, and *d*. Profile *a* in Figure 7(a) (at $V=2.91$ V and $x=0.005$) corresponds to the monoclinic phase and *d* (at $V=2.75$ V and $x=0.084$) predominantly to the tetragonal phase. It was found that all the other x-ray profiles obtained between 2.75 and 2.91 V (x between 0.005 and 0.084) could be expressed by certain combinations of profile *a* and profile *d* in both charge and discharge processes indicating clearly that coexisting phases exist between $x\sim0.01$ and 0.08. Figure 7(b) shows data measured at *a*, *b*, *c*, and *d* and calculations made by combining profiles *a* and *d*. To clearly see the results, only the x-ray profiles for $22°<2\theta<25°$ are plotted. Profile *a* shows the (002), (020), and (200) peaks in the monoclinic phase. In the tetragonal phase only two peaks appear in this region (see profile *d*). The thin solid lines in profile *b* and *c* are the raw experimental data and the thick dashed lines are linear combinations of profiles *a* and *d*. These results prove that Li_xWO_3 undergoes a

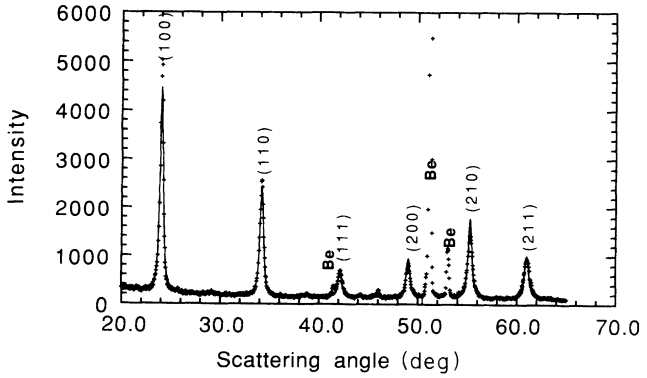

FIG. 6. X-ray-diffraction profile refinement for cubic Li_xWO_3 powder in an x-ray cell at $V=2.0$ V; $x=0.48$ in Li_xWO_3. +++ are the x-ray data and the solid line (——) is the calculated profile. The structure parameters used in the calculation were from Table II. Beryllium peaks were excluded from the calculation.

Table II. Structure parameters for cubic Li_xWO_3 powder. x in Li_xWO_3: 0.48; space group: $Pm3m$; cell dimension: $a_C=3.729$ Å; refined R factor: 0.037; and origin at $m3m$.

	x	y	z	B
W	0.00	0.00	0.00	0.8
O(1)	0.50	0.00	0.00	1.0
O(2)	0.00	0.50	0.00	1.0
O(3)	0.00	0.00	0.50	1.0

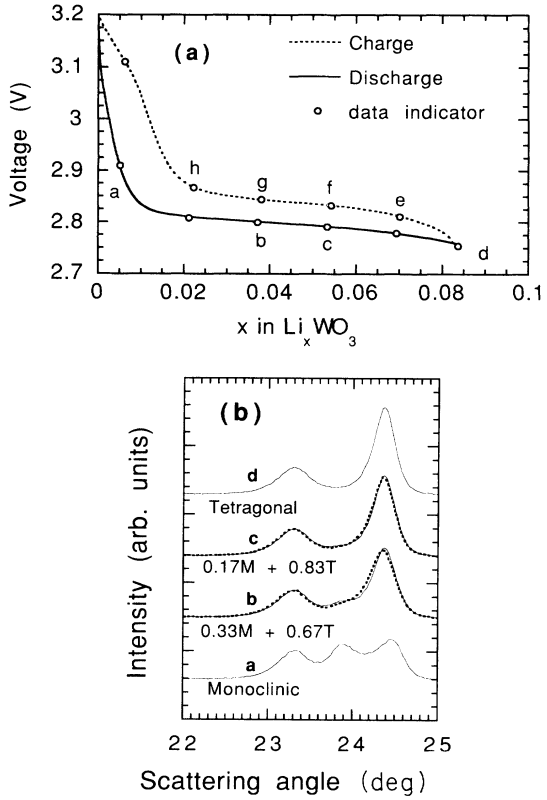

FIG. 7. (a) Voltage vs x for the *in situ* x-ray cell charged and discharged between 3.2 and 2.75 V at a 200-h rate. The variation of x in Li_xWO_3 within each x-ray profile was less than 0.02. The circles on the curves indicate the cell voltage and lithium composition in the Li_xWO_3 in the middle of each x-ray profile. (b) X-ray-diffraction profiles *a*, *b*, *c*, and *d* correspond to circles *a*, *b*, *c*, and *d* in (a). Profile *a* is monoclinic, *d* is tetragonal; profiles *b* and *c* are from the plateau region [see (a)] and can be expressed by linear combination of profiles *a* and *d*. In profiles *b* and *c* the solid curves are raw x-ray data and the dashed curves are from the linear combination of profiles *a* and *d*.

first-order phase transition from the monoclinic phase to the tetragonal phase as Li is intercalculated since coexisting phases are observed.

Using the same methods, we analyzed the x-ray profiles corresponding to the tetragonal ↔ cubic phase transitions. A second *in situ* x-ray experiment was carried out using a constant current corresponding to a 100-h rate. Figure 8(a) shows $V(x)$ measured during discharge and charge for the second *in situ* x-ray cell. The circles on the curves indicate where the x-ray measurements were made. All 40 x-ray profiles were analyzed with the Rietveld profile refinement program. An x-ray profile obtained at $V=2.65$ V and $x=0.1$ [indicated by circle *a* in Fig. 8(a)] showed the tetragonal structure [see pattern *a* in Fig. 8(b)], and the x-ray profile obtained at 2.39 V and $x=0.37$ [indicated by circle *d* in Fig. 8(a)] showed the cubic phase [see profile *d* in Fig. 8(b)]. All (eight) x-ray profiles measured in the tetragonal to cubic phase transition region (from 2.57 to 2.38 V) during the discharge can be expressed by certain linear combinations of tetragonal profile *a* and cubic profile *d*. Figure 8(b) shows calculated profiles for points *b* and *c* collected in the plateau region during discharge as indicated by the circles in Fig. 8(a). The thin solid lines in Fig. 8(b) are the raw x-ray profiles, and the thick dashed lines are suitable linear combinations of profiles *a* and *d*. The linear combinations and the raw data agree well. During charge, the lithium deintercalates from Li_xWO_3. All 11 x-ray patterns from *e'* to *e* in Fig. 8(a) showed cubic crystal structures, but the unit-cell dimension changed continuously. Figure 9 shows the cubic lattice constant plotted vs x in Li_xWO_3 during deintercalation. Figure 9 shows that the volume of cubic unit cell shrinks as lithium is intercalated. The x-ray profiles corresponding to the cubic to tetragonal phase transition during the charge were also analyzed. Circles between *e* and *g* in Fig. 8(a) during the charge were analyzed with the same linear combination method used previously. All x-ray profiles from *e* to *g* could be fitted by a linear combination of profile *a* and profile *e*. All phase transitions in Li_xWO_3 are first order, showing significant coexistence ranges.

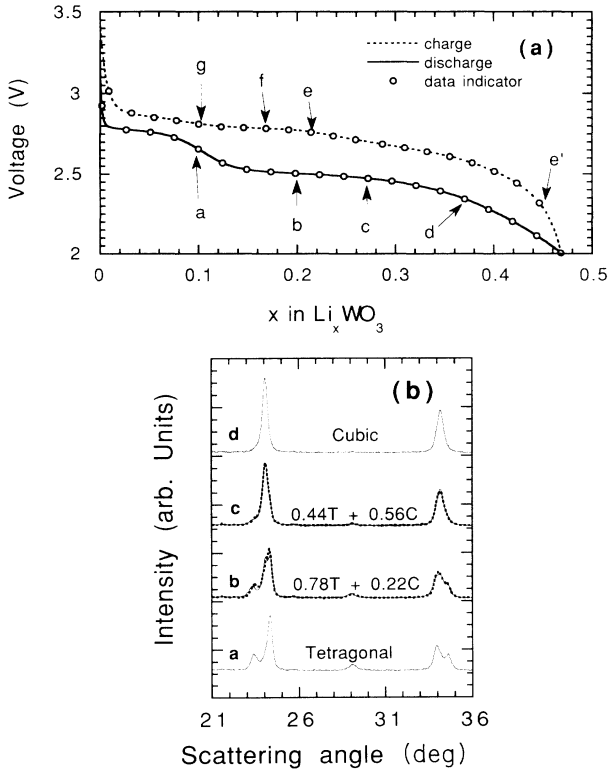

FIG. 8. (a) Voltage vs x for the second *in situ* x-ray cell charged and discharged between 3.2 and 2.0 V at a 100-h rate. Circles on the curves show the state of the x-ray cell in the middle of each x-ray pattern. (b) X-ray profiles *a*, *b*, *c*, and *d* correspond to circles *a*, *b*, *c*, and *d* in (a). Profile *a* is tetragonal and profile *d* is cubic. Profiles *b* and *c* are from the plateau region in discharge and can be expressed by a linear combination of tetragonal profile *a* and cubic profile *d*.

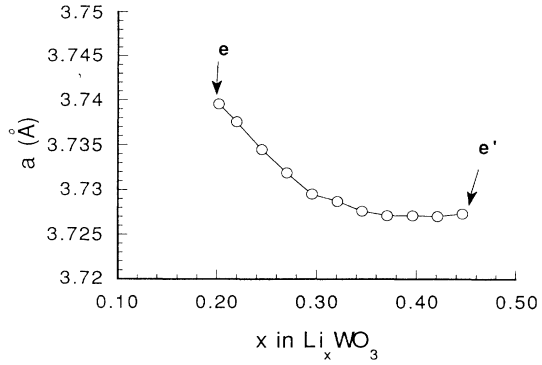

FIG. 9. The cubic unit-cell axis, a_C vs x in Li_xWO_3 during lithium deintercalation in the cubic phase.

Combining all the results discussed above, a phase diagram for electrochemically formed Li_xWO_3 powder at room temperature can be constructed. Figure 10 shows the phase diagram of Li_xWO_3. The phase diagram shows hysteresis between intercalation and deintercalation, especially concerning the range of cubic phase. During discharge (intercalation), Li_xWO_3 is cubic for $0.36<x<0.50$. During charge (deintercalation), Li_xWO_3 is cubic for $0.21<x<0.50$. Figure 9 shows that the cubic lattice constant of Li_xWO_3 during charge is ap-

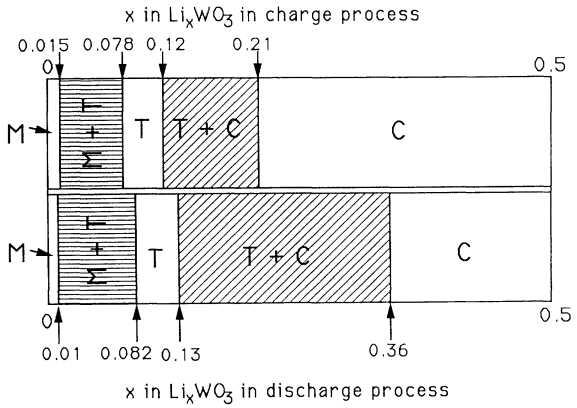

FIG. 10. Phase diagram for electrochemically formed Li_xWO_3 at room temperature.

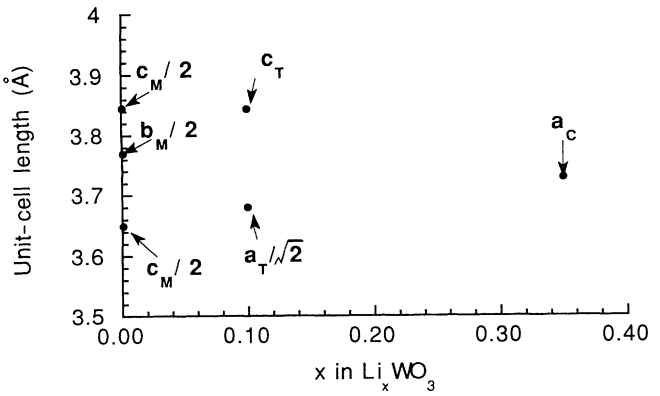

FIG. 11. Comparison of the unit-cell dimensions among three phases.

proximately constant for $0.36<x<0.50$, and then increases as x decreases further. A similar phase diagram for the Li_xWO_3 film is expected, due to the similarities of $V(x)$ and $-dx/dV$.

DISCUSSION AND CONCLUSION

The crystal structures of electrochemically formed Li_xWO_3 and the correspondence of the plateaus of $V(x)$ of the Li/Li_xWO_3 cell with structural transitions were determined. The structures of monoclinic (M), tetragonal (T), and cubic (C) Li_xWO_3 phases are related as shown in Fig. 1 from which the relations of unit-cell dimensions are

$$\begin{aligned} a_M &= 7.310\ \text{Å}\ , \\ b_M &= 7.540\ \text{Å}\ , \\ c_M &= 7.695\ \text{Å}\ , \\ \beta &= 90.89^\circ\ , \end{aligned} \tag{4}$$

$$\begin{aligned} a_T &= 5.203\ \text{Å} \sim \tfrac{1}{2}\sqrt{(a_M^2+b_M^2)}\ , \\ c_T &= 3.844\ \text{Å} \sim \tfrac{1}{2}c_M\ , \end{aligned} \tag{5}$$

$$a_C = 3.729\ \text{Å} \sim (a_M+b_M+c_M)/6 \quad (\text{for } Li_{0.37}WO_3)\ . \tag{6}$$

The WO_3 host is formed by corner-shared WO_6 octahedra extending in three dimensions. The WO_6 octahedra zigzag in the WO_3 structure so a unit cell with eight W atoms must be chosen to show the lattice symmetry.

As lithium intercalates, the structure of the WO_3 host changes first to tetragonal symmetry. The zigzag of the octahedra in the c direction disappears ($c_T=\frac{1}{2}c_M$) and the W-O bond lengths in the a and b directions become equal ($a_T=b_T$). There are two W atoms in the tetragonal unit cell.

TABLE III. The comparison of unit-cell volumes of three phases.

Phase	Unit-cell volume (Å^3)	Comparison (Å^3)
Monoclinic WO_3	$V_M=424.1$	$V_M/8=53.01$
Tetragonal Li_xWO_3	$V_T=104.3$	$V_T/2=52.15$
Cubic Li_xWO_3	$V_C=51.73$	$V_C=51.73$

With more intercalated lithium, the structure of the Li_xWO_3 host finally becomes cubic. The zigzags of the WO_6 octahedra disappear ($a_C \sim \frac{1}{2}a_M$, $\frac{1}{2}b_M$, the $\frac{1}{2}c_M$), the W-O bond length becomes equal in all three directions, and there is a single W atom in the ReO_3-like unit cell. Figure 11 shows comparable unit-cell dimensions: $\frac{1}{2}a_M$, $\frac{1}{2}b_M$, $\frac{1}{2}c_M$, $a_T/\sqrt{2}$, c_T, and a_C for the three structures obtained in Li_xWO_3.

It is worthwhile to compare the unit-cell volumes of the monoclinic (V_M), tetragonal (V_T), and cubic (V_C) phases. Keeping the unit-cell relations in mind (see Fig. 1), we compare the values of $V_M/8$, $V_T/2$, and V_C in Table III. The lattice dimensions of the Li_xWO_3 host shrink as lithium is added. The intercalated lithium atoms are located at interstitial sites (we do not know exactly where they are) and ionized at room temperature. The electron from the Li $2s$ level enters into the conduction band made up predominantly of W $5d$ orbitals. The Li^+ ions at interstitial positions may then attract the surrounding O^{2-} ions in the lattice causing the lattice to contract.

Sleight and Gillson[18] have studied the solid solution series $Re_zW_{1-z}O_3$. They found that, for $z>0.25$, the compound is isostructural with ReO_3, i.e., cubic. Since Re has one more electron than W, this suggests that the charge transfer from Li to WO_3, not the presence of the Li in the lattice, is responsible for the $M \leftrightarrow T \leftrightarrow C$ phase transitions in WO_3. Sleight and Gillson did not investigate small Re concentrations so they did not find a tetragonal phase which may exist.

The charge transfer from Li to the WO_3 host is thought to move the Fermi level upward with respect to the bands in the rigid-band model. The rigid-band model only works well when the host does not change significantly as intercalant is added. As we have shown, the monoclinic phase of Li_xWO_3 is extremely narrow with $0<x<0.01$. Beyond $x=0.01$, coexistence with the tetragonal phase occurs. Therefore, any interpretation of the electrochromic effects which occur in Li_xWO_3 must consider the physical properties of the tetragonal phase and must go beyond a simple interpretation of the rigid-band model.

*To whom correspondence should be sent.

[1]H. R. Zeller and H. U. Beyeler, Appl. Phys. **13**, 231 (1977).
[2]S. K. Mohapatra, J. Electrochem. Soc. **125**, 284 (1978).
[3]B. W. Faughnan and R. S. Crandall, in *Topics in Applied Physics,* edited by J. L. Pankove (Springer-Verlag, Berlin, 1980), Vol. 39, Chap. 5.
[4]I. D. Raistrick, A. J. Mark, and R. A. Huggins, Solid State Ion. **5**, 351 (1981).
[5]J. R. Dahn and W. R. McKinnon, J. Electrochem. Soc. **131**, 1823 (1984).

[6]J. R. Dahn, W. R. McKinnon, and S. T. Coleman, Phys. Rev. B **31**, 484 (1985).
[7]W. R. McKinnon and R. R. Haering, in *Modern Aspects of Electrochemistry,* edited by R. E. White, J. O'M. Bockis, and B. E. Conway (Plenum, New York, 1983), No. 15, p. 235.
[8]J. R. Dahn, M. A. Py, and R. R. Haering, Can. J. Phys. **60**, 307 (1982).
[9]J. R. Dahn, Phys. Rev. B **44**, 9170 (1991).
[10]B. O. Loopstra and H. M. Rietveld, Acta Crystallogr. B **25**, 1420 (1969).
[11]Q. Zhong and J. R. Dahn, J. Electrochem. Soc. (to be published).
[12]J. R. Dahn, R. Fong, and M. J. Spoon, Phys. Rev. B **42**, 6424 (1990).
[13]R. Fong, U. Von Sacken, and J. R. Dahn, J. Electrochem. Soc. **137**, 2009 (1990).
[14]H. M. Rietveld, Acta Crystallogr. **22**, 151 (1967).
[15]H. M. Rietveld, J. Appl. Crystallogr. **2**, 65 (1969).
[16]D. B. Wiles and R. A. Young, J. Appl. Crystallogr. **14**, 149 (1981).
[17]R. J. Hill and C. J. Howard, J. Appl. Cryst. **18**, 173 (1985).
[18]A. W. Sleight and J. L. Gillson, Solid State Commun. **4**, 601 (1966).